Helical twist controls the thickness of F-actin bundles

M. M. A. E. Claessens[†], C. Semmrich[‡], L. Ramos[§], and A. R. Bausch[‡¶]

[†]Mesa+ Institute for Nanotechnology and Biophysical Engineering Group, University of Twente, 7500 AE, Enschede, The Netherlands; [‡]Lehrstuhl für Biophysik E27, Technische Universität München, 85747 Munich, Germany; and [§]Laboratoire des Colloïdes, Verres et Nanomatériaux, UMR CNRS-UM2 5587, Université Montpellier II, 34 095 Montpellier Cedex 5, France

Edited by David R. Nelson, Harvard University, Cambridge, MA, and approved May 7, 2008 (received for review November 26, 2007)

In the presence of condensing agents such as nonadsorbing polymer, multivalent counter ions, and specific bundling proteins, chiral biopolymers typically form bundles with a finite thickness, rather than phase-separating into a polymer-rich phase. Although short-range repulsive interactions or geometrical frustrations are thought to force the equilibrium bundle size to be limited, the precise mechanism is yet to be resolved. The importance of the tight control of biopolymer bundle size is illustrated by the ubiquitous cytoskeletal actin filament bundles that are crucial for the proper functioning of cells. Using an *in vitro* model system, we show that size control relies on a mismatch between the helical structure of individual actin filaments and the geometric packing constraints within bundles. Small rigid actin-binding proteins change the twist of filamentous actin (F-actin) in a concentration-dependent manner, resulting in small, well defined bundle thickness up to ≈20 filaments, comparable to those found in filopodia. Other F-actin cross-linking proteins can subsequently link these small, well organized bundles into larger structures of several hundred filaments, comparable to those found in, for example, *Drosophila* bristles. The energetic tradeoff between filament twisting and cross-linker binding within a bundle is suggested as a fundamental mechanism by which cells can precisely adjust bundle size and strength.

chiral aggregates | finite size | thickness control | cytoskeleton organization

Bundles of filamentous-actin (F-actin) are key components of the eukaryotic cytoskeleton and are generally used for mechanical support. In filopodia, microvilli, and stereocilia, F-actin bundles fortify cellular protrusions, and in stress fibers, they help to maintain cellular integrity. The appearance of parallel F-actin bundles is tightly controlled by a myriad of actin-binding proteins (ABPs). Moreover, cytoskeletal processes that involve F-actin bundles typically employ their own complements of multiple ABPs (1). Although this finding is probably at least partly related to the specific mechanical requirements of the different structures (2, 3), the well defined length, thickness, and organization of the various cytoskeletal F-actin bundles might necessitate the use of a combination of different ABPs. Loss of one of the ABPs typically affects either the organization or thickness of the bundles (1, 4–6), and mutations often result in diseases (7, 8).

In the presence of nonadsorbing polymer and/or multivalent counterions, charged biopolymers such as F-actin, microtubules, or DNA generally form a phase of bundles with a well defined thickness (9–16). The stabilization mechanism of counterion-induced bundles is proposed to be similar to that of colloidal clusters (17, 18); steric and short-range electrostatic interactions or frustration within the bundles prevent charge neutralization and limit the bundle size (19). Alternatively, the finite size of chiral biopolymers has been suggested to result from a buildup of in-plane shear elastic stresses (20), which can result in braided structures (21). Although there are indications that, *in vitro*, the diameter of ABP/F-actin bundles is well defined, reconstructed ABP/actin bundles are typically embedded in a continuous isotropic background network, which has prevented a clear description or quantitative analysis (22, 23). The ABP fascin organizes actin filaments into a cross-linked network of bundles, in which no single filament can be observed (24). This makes a reconstituted F-actin/fascin system ideally suited to resolve the mechanism underlying the finite size of F-actin/ABP bundles.

Here, we investigate the thickness and organization of actin filaments bundled by fascin and show that the helical structure of F-actin and the packing symmetry within the bundle are essential for the control of bundle thickness. F-actin/fascin bundles display a uniform thickness and are straight over long distances, reflecting their high bending rigidity (2). The bundle thickness is independent of the actin concentration and depends exclusively on the molar ratio between bound fascin and G-actin R^*. When the actin concentration is increased at $R^* \approx 1$, a decrease in the number of actin bundles per unit volume, rather than an increase in bundle diameter, is observed (Fig. 1 *A* and *B*). The thickness of the F-actin/fascin bundles is extracted at constant actin concentration from electron micrographs by fitting a Gaussian to the intensity profiles (Fig. 1*C Inset*). The bundle thickness distributions obtained in this way are very uniform and show a slight increase of the bundle diameter, D, with the fascin concentration $D \approx (R^*)^{0.3}$ (Fig. 1*C*). Interestingly, D reaches a plateau at $R^* \approx 0.25$; a further increase of the fascin concentration has no influence on the bundle diameter. The observed thickness of F-actin/fascin bundles is independent of the preparation procedure. Whether long or shortened, filaments are incubated with fascin or fascin already present during the polymerization process does not affect D.

It is not *a priori* clear why bundles with such a well defined diameter are observed or what causes the bundle thickness to be limited. The bundle diameter could, in principle, be either kinetically (25–27) or thermodynamically (19, 20) constrained. However, the independence of the bundle diameter on the preparation method and system used strongly suggests an equilibrium mechanism. Although charge accumulation has been suggested to prevent clusters of charged colloidal particles and counterion-induced F-actin bundles to grow beyond a certain size (19, 28), this is not the case for ABP/F-actin bundles. The separation between F-actin filaments bundled with fascin is ≈5 nm, which is much larger than the Debye length at the ionic strength used. Decreasing the salt concentration to the minimum necessary for actin polymerization (2 mM $MgCl_2$, no KCl or $CaCl_2$) therefore has no influence on the maximum F-actin/fascin bundle thickness. Because electrostatic repulsion between actin filaments is too short-ranged to affect bundle assembly, other mechanisms have to be responsible for preventing bundles from growing thicker.

To precisely quantify the finite and limited thickness of actin bundles, a mesoscopic system is advantageous. The recently intro-

Author contributions: M.M.A.E.C., C.S., L.R., and A.R.B. designed research; M.M.A.E.C., C.S., L.R., and A.R.B. performed research; M.M.A.E.C. and C.S. analyzed data; and M.M.A.E.C., C.S., and A.R.B. wrote the paper.

The authors declare no conflict of interest.

This article is a PNAS Direct Submission.

¶To whom correspondence should be addressed. E-mail: abausch@ph.tum.de.

This article contains supporting information online at www.pnas.org/cgi/content/full/0711149105/DCSupplemental.

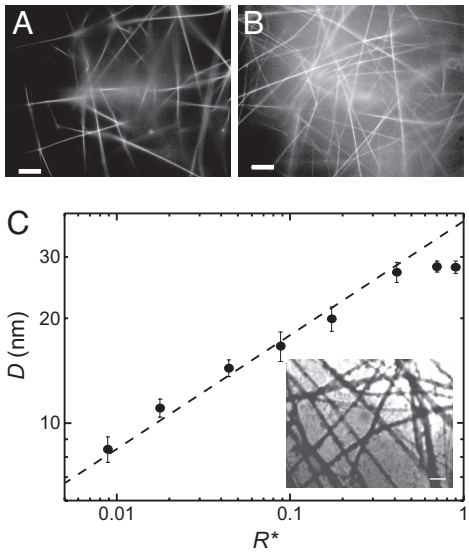

Fig. 1. Finite and limited thickness of F-actin/fascin bundles. (*A* and *B*) Fluorescence micrographs of TRITC phalloidin-labeled actin bundles. The bundles are cross-linked with fascin ($R^* = 1$). Increasing the actin concentration from 0.04 mg/ml (*A*) to 0.1 mg/ml (*B*) merely increases the number of actin bundles per unit volume and seems to have no effect on the bundle thickness. (Scale bars: 10 μm.) (*C*) Bundle diameters *D* obtained from TEM micrographs (*Inset*) as a function of R^* ($c_a = 0.1$ mg/ml).

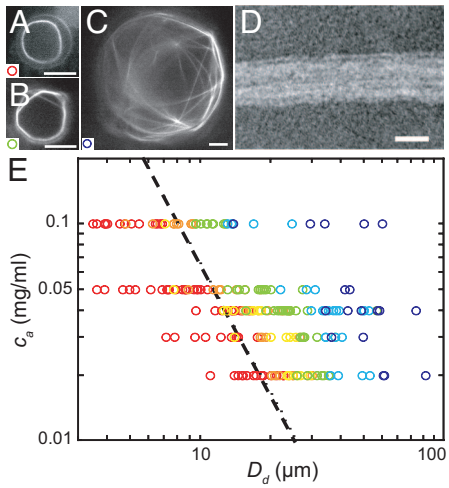

Fig. 2. F-actin fascin bundles in confinement. (*A–C*) Fluorescent micrographs of TRITC phalloidin-labeled F-actin/fascin bundles ($R^* = 1$). For small-droplet diameters filaments organize into a single ring, in larger droplets a second bundle appears, and in very large droplets more complicated structures are found. (Scale bars: 10 μm.) (*D*) TEM micrograph of a detail of an actin bundle obtained from the confined rings showing the typical bundle diameter of ≈5 filaments. (Scale bar: 20 nm.) (*E*) The organization of actin bundles as a function of the actin concentration c_a and emulsion droplet diameter D_d. The colors depicted in the diagram represent the different structures presented in *A–C*. A single bundle does not grow thicker than ≈20 filaments, and the dotted line represents $n_f = 20$.

duced emulsion droplet system seems extremely well suited for this purpose (29). At small-droplet diameters, D_d, F-actin filaments bundle into a single ring in the presence of fascin (2). With increasing droplet diameter, this ring splits into two. In the largest droplets, complicated structures are found (Fig. 2 *A–C*). The total mass of F-actin within a drop or, equivalently, its total length, *L*, can be computed very precisely from the actin concentration and droplet diameter. The bundle radius can be measured, and, for the case of a single ring, the number of filaments (n_f) in the bundle can be deduced. We observe that a confined single bundle does not become thicker than ≈20 filaments (Fig. 2*E*). Instead of growing thicker rings, filaments rather organize into more bundles upon increasing droplet diameter or actin concentration. Transmission electron microscopy (TEM) micrographs of actin rings extracted from emulsion droplets show closely packed F-actin/fascin bundles with a typical diameter of five to six filaments (Fig. 2*D*). Considering the expected hexagonal packing (30), this finding is in excellent agreement with the maximum of ≈20 filaments per bundle estimated from Fig. 2*E*. Therefore, we assume that the plateau in $D(R^*)$ for $R^* > 0.25$ is reached when the bundle contains ≈20 filaments (Fig. 1*C*), which is comparable to those found in filopodia (31).

Considering the observed maximum bundle thickness of ≈20 filaments and the scaling of $D \approx (R^*)^{0.3}$ (Fig. 1*C*), a geometrical argument shows that, for bundles with $n_f < 20$, not all possible cross-linker binding sites are occupied, whereas the maximum size observed experimentally agrees with the full occupation of all possible binding sites [supporting information (SI) *Methods*]. Growth of the bundles is not prevented by a lack of ABPs, but instead seems to be physically limited to two hexagonal shells of actin filaments, which is comparable to those found in filopodia (31).

To investigate the microscopic bundle geometry more closely, we performed Small Angle X-Ray Scattering (SAXS) experiments. Fig. 3*B* shows a typical 2D diffraction pattern of partially aligned F-actin/fascin bundles, and Fig. 3*A* depicts circularly averaged intensities for different R^* values. The appearance of the sharp q_{10} peak at 0.585 nm^{-1} for $R^* > 0.1$ is indicative of bundle formation (Fig. 3*A*). The individual actin filaments in these bundles are packed onto a hexagonal lattice with a center-to-center distance of $4\pi/\sqrt{3}(q_{10}) = 12.4$ nm. Besides the $q_{10}, q_{11} = \sqrt{3}q_{10}, q_{20} = 2q_{10}$, and $q_{21} = \sqrt{7}q_{10}$ peaks characteristic of hexagonal packing, additional peaks due to the helical structure of the F-actin filaments appear along q_z (Fig. 3*A*). In the absence of fascin, the actin filament displays a −13/6 symmetry (13 monomers and 6 helical turns per crystallographic repeat) characterized by broad diffraction peaks at 1.14 and 1.25 nm^{-1}. These peaks correspond to the sixth and seventh layer lines ($n = 1$ and $n = -1$ Bessel functions), which are much more intense than the other layer lines and dominate the diffraction pattern of partially aligned F-actin. In F-actin bundles, this layer line pattern is convoluted with the hexagonal bundle structure, resulting in a splitting up in different sharp peaks along q_z (32). The position of these peaks gradually shifts with increasing fascin concentration until at $R^* > 0.25$ the peaks appear at 1.20, 1.35, and 1.46 nm^{-1} (Fig. 3*A*), indicating a change in twist. The filament twist is extracted by fitting the four-sphere model (33) to the diffraction pattern of hexagonal bundles at $R^* > 0.03$ (Fig. 3*C*). With increasing fascin concentration, the helical symmetry gradually changes from the original −13/6 to an overtwisted −28/13 symmetry. The maximum overtwist of ≈1° per actin monomer (Fig. 3*D*) is comparable with the overtwist observed for F-actin/espin bundles (32).

Although the width of the twist probability distribution observed for single-actin filaments is quite broad (34), fixing the filaments in a new overtwisted position costs energy. The energetic cost involved in overtwisting F-actin will have to be provided for by fascin binding. The twist energy can be obtained for each value of R^* from the torsional stiffness $\tau = 810^{-26}$ Nm^2 (35), actin monomer spacing ($d = 2.9$ nm), and the observed increase in overtwist $\Delta\theta$: $E_{twist} = \tau(\Delta\theta)^2 d^{-1}$. The calculated E_{twist} is found to be constant per bound fascin. For all fascin and actin concentrations, the gain in binding energy per actin monomer is slightly larger than the loss in torsional energy per actin monomer. The energy necessary for twisting turns out to be ≈10k_BT

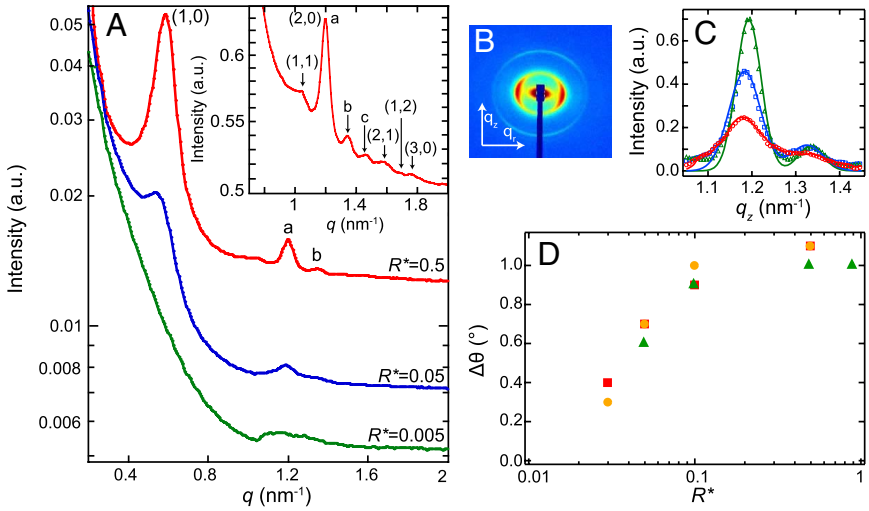

Fig. 3. Microscopic bundle geometry. (*A*) Circularly averaged diffraction data for different R^* values and $c_a = 2$ mg/ml. For $R^* \geq 0.01$, peaks related to hexagonal packing of filaments appear. (*Inset*) A magnification of the diffraction at $R^* = 0.5$ is shown. The peaks belonging to the helical symmetry are indexed as a, b, and c. (*B*) A typical 2D diffraction pattern of a partially aligned F-actin/fascin network obtained by SAXS experiments for $R^* = 0.5$ and $c_a = 2$ mg/ml. (*C*) Angularly averaged wedges along the axial direction q_z. Peaks corresponding to the helical structure of the actin filaments shift with R^*. The continous lines are fits to the data (open circle, $R^* = 0.05$; open square, $R^* = 0.1$; filled triangle, $R^* = 0.5$). (*D*) The change in overtwist obtained from the diffraction pattern as a function of both fascin (R^*) and actin concentrations (filled triangle, $c_a = 0.8$ mg/ml; filled square, $c_a = 2$ mg/ml; filled circle, $c_a = 3$ mg/ml).

per bound fascin, whereas fascin binding provides $\Delta G = k_B T \ln(K_D) \approx 15\ k_B T$ per bound fascin molecule (36).

In the original $-13/6$ helical symmetry of individual actin filaments, possible fascin-binding sites are not separated by exactly 60°. Therefore, F-actin is not ideally suited for hexagonal packing (11, 30). To fit the filaments on a hexagonal lattice, ABPs have to twist or locally stretch the F-actin. The $-28/13$ symmetry observed for the saturated F-actin/fascin bundles is still suboptimal for hexagonal packing, and bundle thickness is therefore given by the total number of bound fascin (*SI Methods*). Because the number of fascin-binding sites along an actin filament is limited, the bundles cannot grow beyond a thickness of ≈20 filaments. This mechanism provides a molecular explanation for the finite sizes observed for F-actin bundled in the presence of ABPs or condensing agents *in vitro* (10–12, 22).

However, in contrast to what has been observed *in vitro*, bigger bundles consisting of hundreds of actin filaments are found in several cytoskeletal processes (1, 4, 5). Interestingly genetic mutations have shown that these thick F-actin bundles are typically linked by more than one APB species. Indeed, *in vitro*, the use of an additional ABP with a different actin-binding site also results in larger structures (Fig. 4). In the presence of the ABPs α-actinin or espin, small F-actin/fascin bundles organize into thick bundles of several hundred filaments (Fig. 4). The limited number of binding sites and the flexibility of the additional linker ABP will again limit the thickness of these thick bundles. The control of bundle thickness by the helical twist and filament packing constraints gives an explanation for the use of multiple ABPs in one bundle. Because fascin gives rise to well organized but rather thin bundles, additional ABPs are required to link these bundles in larger structures, as was observed in, for example, *Drosophila* bristles previously (4).

Thus, it seems that nature deliberately chose to have a mismatch between the pitch of individual helical polymers and the optimum value required for hexagonal packing to implement an intrinsic limit to bundle growth as observed in microvilli, filopodia, and stereocilia. Moreover, the helical structure of actin filaments is affected by several ABPs (30, 32, 37, 38), suggesting that this conformational variability of F-actin is exploited in many cytoskeletal processes. By adapting the twist, tilt, and rotation of actin filaments in the acrosomal bundle, the ABP scruin is thought to store energy in the actin helix that can subsequently be used in the acrosomal process (37, 39).

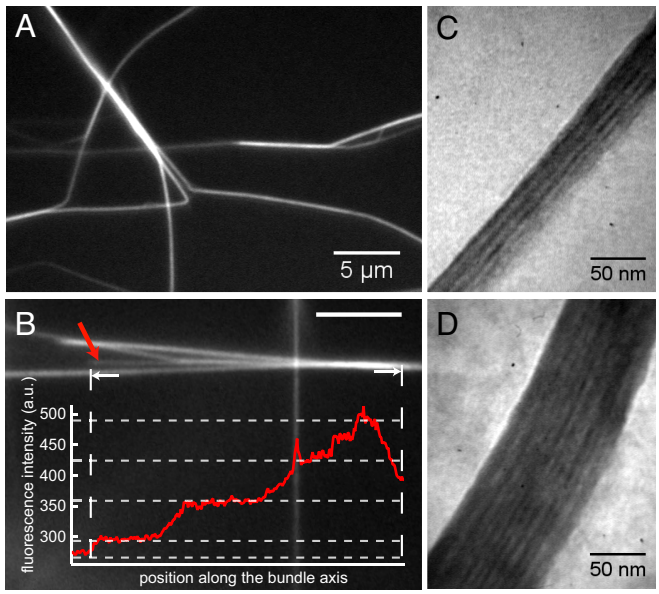

Fig. 4. Combination of different ABPs. (*A–D*) Fluorescence (*A* and *B*) and EM (*C* and *D*) micrographs of actin bundles. In the presence of α-actinin (*B*) or espin (*A*), small fascin/actin bundles ($R_{fascin} = 1$) can be linked into thicker ones. The ends of these bundles sometimes look frayed, showing that the bundle consists of many smaller bundles. The smaller bundles are straight over long-length scales, reflecting their large bending rigidity compared to single-actin filaments. The fluorescence intensity profile along the bundle indicated with the red arrow shows several steps, indicating that the final bundle consists of approximately seven smaller ones. (*C*) In the presence of WT human espin, actin filaments are organized into bundles with a well defined thickness, compared with those observed in the presence of fascin ($c_a = 0.95\ \mu$M, $R_{espin} = 4$). (*D*) In the presence of both fascin and espin, much thicker bundles are formed ($c_a = 0.95\ \mu$M, $R_{espin} = 4$, $R_{fascin} = 1$). The bundle shown in *D* has a diameter that is approximately three times that of a fascin or espin bundle, equivalent to 100–200 filaments.

In conclusion, we have shown that the geometric constraints imposed by the helical structure of actin filaments are exploited to tightly control bundle thickness. The balance between mechanical twisting energy costs and gains in binding energy regulates actin bundle formation and growth. Besides twisting the filaments in the bundle, mechanical strain involved in bundling chiral polymers also can, in principle, result in a supertwist of the bundles affecting the resulting functional structures (20, 40). The supercoiling observed for filamin/actin bundle rings in vesicles might be a first indication that there are indeed some ABPs that supertwist the whole bundle, rather than overtwist the individual filaments (41). Superhelical bundles probably writhe to release strain in the filaments and ABPs, giving rise to supertwisted than superhelical bundles. Moreover, the twisted structure of chiral bundles also could be the source of torque observed in *Listeria* movements (42) and might give insight into the molecular origin of helical structures observed for carbon nanotubes (43).

Methods

Lyophilized G-actin from rabbit skeletal muscle (44) was dissolved in deionized water, dialyzed against G-buffer [2 mM Tris, 0.2 mM ATP, 0.2 mM $CaCl_2$, 0.2 mM DTT, and 0.005% NaN_3 (pH 8)], stored at 4°C, and used within 7 days after preparation. Recombinant human fascin and espin were expressed in *Escherichia coli* BL21-codon$^+$ bacteria as described previously (2, 36, 45). F-actin/fascin networks were constructed by polymerizing G-actin in the presence of fascin in F-buffer [2 mM Tris, 0.5 mM ATP, 0.2 mM $CaCl_2$, 2 mM $MgCl_2$, 100 mM KCl, and 0.2 mM DTT (pH 7.5)] at 20°C. For fluorescence microscopy, F-actin filaments were fluorescently labeled by using TRITC-phalloidin. Emulsion droplets containing F-actin/fascin bundles were prepared as described previously (2, 29). Samples for TEM (Philips EM400T) were adsorbed to glow-discharged, carbon-coated formvar films on copper grids and negatively stained with 0.8% uranyl acetate; Excess liquid was then drained with filter paper. To be able to compare experiments performed at different actin concentrations, the molar ratio, R, between fascin and actin, $R = c_f/c_a$, was translated into an effective R^*, assuming an equilibrium dissociation constant $K_d = 0.3\ \mu$M (36) and $R^* = \frac{1}{2}((1 + R + K_d/c_a) - ((1 + R + K_d/c_a)^2 - 4R)^{1/2})$. Deviations of R^* from R become apparent at high R or low-actin concentrations.

Synchrotron small-angle x-ray experiments were performed on the ID-2 beam line at the European Synchrotron Radiation Facility (Grenoble, France). For these experiments, F-actin/fascin networks were polymerized in 1.5-mm quartz capillaries at actin concentrations between 0.8 and 5 mg/ml. These samples showed powder scattering; to be able to discern correlations between different directions, the actin bundles were partially aligned by using a flow cell. The scattering was done at 12.46 keV and a sample to-detector distance of 1 m. Scans were performed for 0.5–6 s; during this time period, no radiation damage was observed. The diffraction data were analyzed by using the program EDF plot (46). Control experiments showed that the phalloidin labeling used in fluorescence experiments does not affect the filament twist.

ACKNOWLEDGMENTS. We thank M. Rusp for the actin preparation; D. Vignjevic (Institut Curie, Paris) for the kind gift of recombinant fascin plasmids; J. Bartles (Northwestern University, Feinberg School of Medicine, Chicago) for providing the espin plamid; E. Di Cola for help with the SAXS experiments; and K. Purdy, K. Kroy, R. Netz, and H. Wada for interesting and insightful discussions. This work was supported by Deutsche Forschungsgemeinschaft through the DFG-Cluster of Excellence Munich-Centre for Advanced Photonics (MAP), the Nanosystems Initiative Munich (NIM) and by the SFB413.

1. Bartles JR (2000) Parallel actin bundles and their multiple actin-bundling proteins. *Curr Opin Cell Biol* 12:72–78.
2. Claessens MMAE, Bathe M, Frey E, Bausch AR (2006) Actin-binding proteins sensitively mediate F-actin bundle stiffness. *Nat Mater* 5:748–753.
3. Bathe M, *et al*. (2008) Cytoskeletal bundle mechanics. *Biophys J* 94:2955–2964.
4. Tilney LG, *et al*. (1998) Why are two different cross-linkers necessary for actin bundle formation *in vivo* and what does each cross-link contribute? *J Cell Biol* 143:121–133.
5. Tilney LG, *et al*. (2000) Regulation of actin filament cross-linking and bundle shape in *Drosophila* bristles. *J Cell Biol* 148:87–99.
6. Guild GM, *et al*. (2005) Actin filament bundles in *Drosophila* wing hairs: Hairs and bristles use different strategies for assembly. *Mol Biol Cell* 16:3620–3631.
7. Cant K, Knowles BA, Mooseker MS, Cooley L (1994) *Drosophila* singed, a fascin homolog, is required for actin bundle formation during oogenesis and bristle extension. *J Cell Biol* 125:369–380.
8. Zheng LL, *et al*. (2000) The deaf jerker mouse has a mutation in the gene encoding the espin actin-bundling proteins of hair cell stereocilia and lacks espins. *Cell* 102:377–385.
9. Tang JX, Janmey PA (1996) The polyelectrolyte nature of F-actin and the mechanism of actin bundle formation. *J Biol Chem* 271:8556–8563.
10. Hosek M, Tang JX (2004) Polymer-induced bundling of F actin and the depletion force. *Phys Rev E* 69:051907.
11. Angelini TE, Liang H, Wriggers W, Wong GCL (2003) Like-charge attraction between polyelectrolytes induced by counterion charge density waves. *Proc Natl Acad Sci USA* 100: 8634–8637.
12. Lai GH, *et al*. (2007) Evolution of growth modes for polyelectrolyte bundles. *Phys Rev Lett* 98:187802.
13. Tharmann R, Claessens MMAE, Bausch AR (2006) Micro- and macrorheological properties of actin networks effectively crosslinked by depletion forces. *Biophys J* 90: 2622–2627.
14. Needleman DJ, *et al*. (2004) Higher-order assembly of microtubules by counterions: From hexagonal bundles to living necklaces. *Proc Natl Acad Sci USA* 101:16099–16103.
15. Conwell CC, Vilfan ID, Hud NV (2003) Controlling the size of nanoscale toroidal DNA condensates with static curvature and ionic strength. *Proc Natl Acad Sci USA* 100: 9296–9301.
16. Bloomfield VA (1997) DNA condensation by multivalent cations. *Biopolymers* 44:269–282.
17. Segre PN, Prasad V, Schofield AB, Weitz DA (2001) Glasslike kinetic arrest at the colloidal-gelation transition. *Phys Rev Lett* 86: 6042–6045.
18. Stradner A, *et al*. (2004) Equilibrium cluster formation in concentrated protein solutions and colloids. *Nature* 432:492–495.
19. Henle ML, Pincus PA (2005) Equilibrium bundle size of rodlike polyelectrolytes with counterion-induced attractive interactions. *Phys Rev E* 71:060801.
20. Grason G, Bruinsma R (2007) Chirality and equilibrium biopolymer bundles. *Phys Rev Lett* 99:098101.
21. Ikawa T, *et al*. (2007) Molecular scale imaging of F-actin assemblies immobilized on a photopolymer surface. *Phys Rev Lett* 98:018101.
22. Wagner B, *et al*. (2006) Cytoskeletal polymer networks: The molecular structure of cross-linkers determines macroscopic properties. *Proc Natl Acad Sci USA* 103:13974–13978.
23. Bausch AR, Kroy K (2006) A bottom-up approach to cell mechanics. *Nat Phys* 2:231–238.
24. Lieleg O, *et al*. (2007) Mechanics of bundled semiflexible polymer networks. *Phys Rev Lett* 99:088102.
25. Ha BY, Liu AJ (1999) Kinetics of bundle growth in DNA condensation. *Europhys Lett* 46:624–630.
26. Kierfeld J, Kuhne T, Lipowsky R (2005) Discontinuous unbinding transitions of filament bundles. *Phys Rev Lett* 95:038102.
27. Haviv L, Gov N, Ideses Y, Bernheim-Groswasser A (2008) Thickness distribution of actin bundles in vitro. *Eur Biophys J* 37:447–454.
28. Groenewold J, Kegel WK (2001) Anomalously large equilibrium clusters of colloids. *J Phys Chem B* 105:11702–11709.
29. Claessens MMAE, Tharmann R, Kroy K, Bausch AR (2006) Microstructure and viscoelasticity of confined semiflexible polymer networks. *Nat Phys* 2: 186–189.
30. DeRosier DJ, Tilney LG (1981) How actin-filaments pack into bundles. *Cold Spring Harb Symp Quant Biol* 46:525–540.
31. Svitkina TM, et al. (2003) Mechanism of filopodia initiation by reorganization of a dendritic network. *J Cell Biol* 160:409–421.
32. Purdy KR, Bartles JR, Wong GCL (2007) Structural polymorphism of the actin-espin system: A prototypical system of filaments and linkers in stereocilia. *Phys Rev Lett* 98:058105.
33. Al-Khayat HA, Yagi N, Squire JM (1995) Structural-changes in actin-tropomyosin during muscle regulation: Computer modeling of low-angle x-ray diffraction data. *J Mol Biol* 252:611–632.
34. Egelman EH, Francis N, Derosier DJ (1982) F-actin is a helix with a random variable twist. *Nature* 298: 131–135.
35. Tsuda Y, Yasutake H, Ishijima A, Yanagida T (1996) Torsional rigidity of single actin filaments and actin–actin bond breaking force under torsion measured directly by *in vitro* micromanipulation. *Proc Natl Acad Sci USA* 93:12937–12942.
36. Ono S, *et al*. (1997) Identification of an actin binding region and a protein kinase C phospkorylation site on human fascin. *J Biol Chem* 272:2527–2533.
37. DeRosier D, Tilney L, Flicker P (1980) Change in the twist of the actin-containing filaments occurs during the extension of the acrosomal process in limulus sperm. *J Mol Biol* 137:375–389.
38. Stokes DL, DeRosier DJ (1987) The variable twist of actin and its modulation by actin-binding proteins. *J Cell Biol* 104:1005–1017.
39. Schmid MF, Sherman MB, Matsudaira P, Chiu W (2004) Structure of the acrosomal bundle. *Nature* 431:104–107.
40. Kamien RD, Nelson DR (1995) Iterated moire maps and braiding of chiral polymer crystals. *Phys Rev Lett* 74:2499–2502.
41. Limozin L, Sackmann E (2002) Polymorphism of cross-linked actin networks in giant vesicles. *Phys Rev Lett* 89:168103.
42. Shenoy VB, Tambe DT, Prasad A, Theriot JA (2007) A kinematic description of the trajectories of *Listeria monocytogenes* propelled by actin comet tails. *Proc Natl Acad Sci USA* 104:8229–8234.
43. Amelinckx S, *et al*. (1994) A formation mechanism for catalytically grown helix-shaped graphite nanotubes. *Science* 265:635–639.
44. Spudich JA, Watt S (1971) Regulation of rabbit skeletal muscle contraction. 1. Biochemical studies of interaction of tropomyosin–troponin complex with actin and proteolytic fragments of myosin. *J Biol Chem* 246:4866–4871.
45. Bartles JR, *et al*. (1998) Small espin: A third actin-bundling protein and potential forked protein ortholog in brush border microvilli. *J Cell Biol* 143:107–119.
46. Sztucki N, Narayanan, T (2007) Development of an ultra-small-angle x-ray scattering instrument for probing themicrostructure and the dynamics of soft matter. *J Appl Crystallogr S* 40:459–462.